Particle Accelerators
1974, Vol. 6, pp. 19–26

EFFECT OF BEAM WIDTH ON THE INCOHERENT ν-SHIFT DUE TO IMAGE FORCES†

M. MONTH
Brookhaven National Laboratory, Upton, New York 11973, USA
and
R. L. GLUCKSTERN‡
University of Massachusetts, Amherst, Massachusetts 01002, USA

The effect of the distribution of charge in a beam of particles on the space-charge ν-shift is considered. At high energy, the major contribution to the space-charge ν-shift comes from the image fields created by the presence of metallic and ferromagnetic boundaries. For beams small with respect to chamber and magnet dimensions, a point source treatment of the beam is adequate. However, when the beam width is comparable to or greater than the chamber height, the distribution of charge cannot be neglected. To study this effect, a rectangular geometry is used. A conducting vacuum chamber, a parallel plate ferromagnetic surface and a coasting ribbon beam are assumed. It is found that for a large beam size, a, relative to chamber height, h (or magnet gap, g), the image-tune-shift has a $1/ah$ asymptotic behavior, and not $1/a^2$, which might appear to be reasonable from image source arguments. The nonuniformity of the ν-shift along the beam is also considered in detail. It is interesting that the unexpected appearance of the transverse resistive wall instability in the CERN ISR, the 'brickwall' effect, has been attributed to such a condition in the stacked beam. Finally, numerical computations are performed in order to demonstrate the influence on the image-tune-shift of (1) the chamber sidewalls, and (2) the rate of fall-off of the horizontal charge density distribution. It is found that the main effect of bringing the sidewalls near the beam and/or softening the fall-off of the charge density distribution is an increase in the spread of ν-shifts across the horizontal width of the beam.

1. INTRODUCTION

In the original calculations[1] of the space-charge ν-shift, it was pointed out by Laslett that at high energy the major contribution came from image fields, which are due to the presence of metallic and ferromagnetic boundaries. It was recognized that the relevant parameters were chamber and magnet dimensions. Accordingly the beam was treated as a point source. Thus, it is found that the vertical ν-shift is inversely proportional to the square of the vertical chamber height (or magnet gap).

However, it is apparent that as the beam spreads out horizontally, the space-charge shift of the betatron frequency due to images must diminish. This follows if one considers the limit of an infinitely wide beam in a parallel plate geometry. We will see that in this limit the image ν-shift does indeed fall to zero. For the metallic boundary image field, since the electric field produced by the beam is normal, the boundary condition is automatically satisfied and thus the image field vanishes.

We are therefore led to consider the effect of the beam width on the vertical incoherent ν-shift. There are two distinct effects which are taken into account. First, the beam width reduces the effective current at the beam center. This is essentially true all along the beam. The consequence is an overall reduction of the ν-shift. We find that, in fact, if the beam width, a, is sufficiently large compared to the vertical chamber height, h, then the vertical ν-shift due to electric images becomes essentially proportional to $1/a^2$ rather than $1/h^2$, while the ν-shift due to the magnetic image field has a slower drop-off, being proportional to $1/ag$ rather than $1/g^2$ (g is the magnet gap). Secondly, since the image fields vary along the beam, the ν-shift is not uniform. The importance of such a nonuniform incoherent ν-shift in determining the transverse stability of a beam has been recognized. In fact, the 'brickwall effect', which is just the transverse resistive wall instability in the ISR, has been attributed[2,3] to such a condition in the stacked beam.

We will consider a geometry suitable for narrow

†Work performed under the auspices of the US Atomic Energy Commission.
‡Supported in part by the National Science Foundation.

gap magnets, such as used in the ISR or in the design of a 'warm', i.e., nonsuperconducting, magnet for the ISA project.[4] Specifically, we will use an idealized situation consisting of a coasting ribbon beam in a rectangular boundary. A sketch is shown in Figure 1. We assume a conducting vacuum chamber. The ferromagnetic boundary

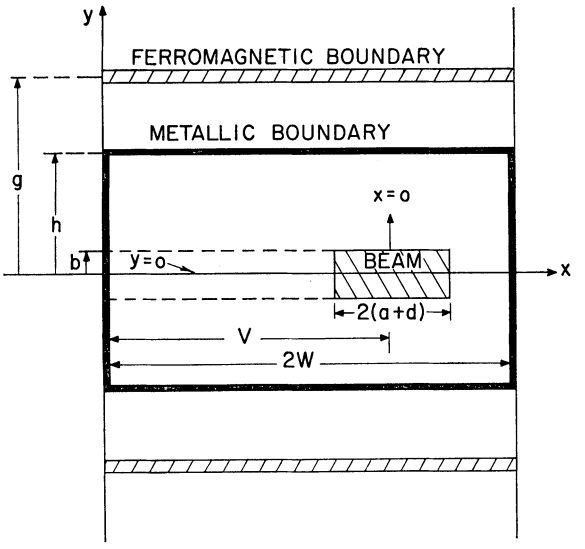

FIGURE 1 Beam and chamber cross section. The parameters are defined in Section 2 of the text.

exists only in the vertical dimension. The horizontal charge density is arbitrary, while vertically, the beam has zero size (i.e., a ribbon beam).

Gluckstern[5] has looked into these effects, and has estimated the v-shift across the beam. However, he only computed the electric image forces and used a point source. Zotter[2] included a source of nonzero size, but he did not show the detailed v-variation along the beam width. We will extend Zotter's analysis, giving the v-variation due to both electric and magnetic image forces. We will show how the beam width becomes a significant parameter in determining the v-shift, how the closeness of the horizontal chamber walls enters, and how the horizontal density function plays a significant role.

2. THE IMAGE TUNE SHIFT

We assume a ribbon beam centered[6] vertically and we will compute the vertical v-shift of a particle oscillating in this beam. There is, of course, the tacit assumption that the charge distribution is fixed. This will give us the incoherent vertical space-charge v-shift.

We will write an expression for the force on a particle in the beam at position x, horizontally, and y, vertically. The coordinates with respect to beam and chamber are defined in Figure 1. We assume that the beam has a uniform charge density vertically and a normalized horizontal density distribution depicted in Figure 2 and given by

$$\sigma(x) = \begin{cases} (2a+d)^{-1} \sin^2\left[\dfrac{\pi}{2}\left(\dfrac{a+d-x}{d}\right)\right], \\ \qquad a \leqq x \leqq (a+d) \\ (2a+d)^{-1}, \qquad -a \leqq x \leqq a \\ (2a+d)^{-1} \sin^2\left[\dfrac{\pi}{2}\left(\dfrac{a+d+x}{d}\right)\right], \\ \qquad -(a+d) \leqq x \leqq -a, \end{cases} \tag{2.1}$$

where x is measured with respect to the beam center, a is the half-width of the constant part of the density function, d is the total width of each flank, and the normalization condition is

$$\int_{\text{beam}} \sigma(x)\,dx = 1. \tag{2.2}$$

To find the force on a particle due to the beam we will use a Fourier decomposition of the fields. We thus require the Fourier coefficients for the beam distribution. Using a chamber width, $2W$, as in Figures 1 and 2, we write

$$\sigma(x) = \frac{1}{W} \sum_{s=1}^{\infty} (g_s \cos \eta x + g_s' \sin \eta x), \tag{2.3}$$

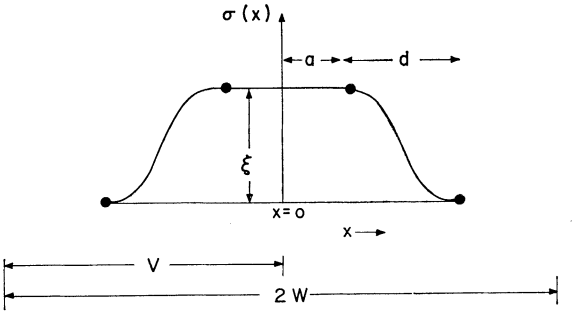

FIGURE 2 Normalized charge density distribution, $\sigma(x)$, in a chamber of width, $2W$. The flanks have $\sin^2$ behavior. The height, ξ, is $1/(2a+d)$. The function is expressed analytically in (2.1) of the text.

where

$$\eta = \frac{\pi}{2}\frac{s}{W}, \tag{2.4}$$

$$g_s = G_s \sin^2 \eta V, \tag{2.5}$$

$$g_s' = G_s \sin \eta V \cos \eta V, \tag{2.6}$$

$$G_s = \frac{\sin \eta(a+\frac{1}{2}d)}{\eta(a+\frac{1}{2}d)} \frac{\cos \frac{1}{2}\eta d}{1-(\eta d/\pi)^2}, \tag{2.7}$$

and V is the position of the beam center in the chamber. For a horizontally centered beam, $V = W$, and thus

$$\begin{aligned} g_s' &= 0, \\ g_s &= 0, \quad s \text{ even}, \\ g_s &= G_s, \quad s \text{ odd}. \end{aligned} \tag{2.8}$$

In this case, the force, F_y, is given by[7]

$$\frac{\varepsilon_0}{e\lambda}\frac{F_y}{y} = \frac{1}{2bW}\sum_{s\,\text{odd}} G_s \left\{ \frac{1}{\gamma^2} e^{-\eta b} + [(1-\tanh \eta h) + \beta^2(\coth \eta g - 1)] \sinh \eta b \right\} \frac{\sinh \eta y}{\eta y} \cos \eta x, \tag{2.9}$$

where h is the half-height of the chamber,
g is the half-gap of the magnet,
γ is the energy in units of proton mass,
β is the particle velocity in units of c,
λ is the linear charge density of the beam,
and b is the beam half-height (we will set $b \to 0$ later).

The force is made up of two components, due to self-fields and due to image fields. The image force arises because of the presence of the metallic and ferromagnetic boundaries; while the self-force is induced by the beam itself and is independent of the boundaries. The self-force can be extracted by allowing the boundaries to move to infinity. The limit $W \to \infty$ changes the sum to an integral. Thus, setting

$$(\pi/2)(2/W) \to dq, \quad (\pi/2)(s/W) \to q, \tag{2.10}$$

we have for the self-force, with $h \to \infty$, $g \to \infty$ and $W \to \infty$

$$\frac{\varepsilon_0}{e\lambda}\frac{F_y}{y} = \frac{1}{2\pi b\gamma^2}\int_0^\infty dq\, G(q)\, e^{-bq} \frac{\sinh qy}{qy} \cos qx. \tag{2.11}$$

The image force can then be found by subtracting the self-force from the total force; that is,

$$F_y^{\text{im}} = F_y - F_y^{\text{self}}. \tag{2.12}$$

For beams of small vertical extent the dominant fields are the gradient ones. Thus, by evaluating the forces near $y = 0$, we can write a vertical v-shift due to space charge,[1]

$$\Delta v = -\frac{N r_p R}{v\beta^2\gamma}\left[\frac{\varepsilon_0}{e\lambda}\frac{F_y}{y}(y=0)\right], \tag{2.13}$$

where N is the total number of particles in the beam (N is related to λ by $\lambda = eN/2\pi R$),
R is the average radius of the ring,
v is the vertical tune,
and r_p is the classical proton radius ($r_p = 1.54 \times 10^{-18}$ m).

In particular, we can express the image contributions to the v-shift as

$$(\Delta v)_{\text{im}} = -\frac{N r_p R}{\pi v\beta^2\gamma}\left[\frac{\varepsilon_1}{h^2} f_1(\alpha, \delta, \omega, t) + \frac{\beta^2\varepsilon_2}{g^2} f_2(\alpha', \delta', \omega', t')\right]. \tag{2.14}$$

Here, ε_1 and ε_2 are the image coefficients defined in Ref. 1 for infinite W—i.e., $\varepsilon_1 = \pi^2/48$, $\varepsilon_2 = \pi^2/24$. f_1 and f_2 are dimensionless form factors. For the electric form factor, f_1, we define dimensionless variables with respect to the chamber half-height, h. We have therefore,

$$\alpha = a/h, \ \delta = d/h, \ \omega = h/W, \ t = x/h. \tag{2.15}$$

In the magnetic form factor, the variables are

$$\alpha' = a/g, \ \delta' = d/g, \ \omega' = g/W, \ t' = x/g. \tag{2.16}$$

We have suppressed the dependence on the beam height, b, since we will take the limit $b \to 0$.

With (2.9) and (2.11) we can thus write

$$(\Delta v)_{\text{im}} = -\frac{N r_p R\pi}{48 v\beta^2\gamma h^2}\left[f_1(\alpha, \delta, \omega, t) + \frac{2\beta^2 h^2}{g^2} f_2(\alpha', \delta', \omega', t')\right], \tag{2.17}$$

where

$$f_1 = \frac{24}{\pi}\omega \sum_{\text{odd}\,s} \tau G_s \cos \tau t (1 - \tanh \tau) + \Delta f(\alpha, \delta, \omega, t), \tag{2.18}$$

$$f_2 = \frac{12}{\pi}\omega' \sum_{\text{odd}\,s} \tau' G_s \cos \tau' t' (\coth \tau' - 1) - \tfrac{1}{2}\Delta f(\alpha', \delta', \omega', t'), \tag{2.19}$$

and

$$\tau = \eta h,\ \tau' = \eta g. \tag{2.20}$$

The quantity Δf is given by

$$\Delta f(\alpha, \delta, \omega, t) = \lim_{\varepsilon \to 0} \frac{24}{\pi\varepsilon}\left\{\omega \sum_{\text{odd } s} G_s \cos \tau t\, e^{-\tau\varepsilon} - \frac{1}{\pi} \times \int_0^\infty dp\, G(p) \cos pt\, e^{-p\varepsilon}\right\}, \tag{2.21}$$

where

$$G(p) = \frac{\sin p(\alpha+\frac{1}{2}\delta)}{p(\alpha+\frac{1}{2}\delta)} \frac{\cos \frac{1}{2}p\delta}{1-(p\delta/\pi)^2}. \tag{2.22}$$

Although the form of Δf given in (2.21) is well defined, both the sum and integral converge very slowly in the limit of small ε. However in this limit, we can obtain a much simpler expression.

Since G_s and $G(p)$ can be written as

$$G_s = \int_{-(\alpha+\delta)}^{\alpha+\delta} dq\, \sigma(q) \cos \tau q, \tag{2.23}$$

and

$$G(p) = \int_{-(\alpha+\delta)}^{\alpha+\delta} dq\, \sigma(q) \cos pq, \tag{2.24}$$

where $\sigma(q)$ is the same as the function defined in (2.1) except that the lengths are in units normalized to h, then (2.21) can be reduced to

$$\Delta f(\alpha, \delta, \omega, t) = -\frac{6}{\pi^2}\omega^2 \int_{-\alpha-\delta}^{\alpha+\delta} dq\, \sigma(q)\left[\frac{1}{A^2} - \frac{\pi^2 \cos \pi A}{\sin^2 \pi A}\right], \tag{2.25}$$

where

$$A = \tfrac{1}{2}\omega(q-t). \tag{2.26}$$

This integral is easily performed numerically.

3. ANALYTICAL RESULTS IN THE CASE OF NO SIDEWALLS

The case of no sidewalls, i.e., parallel plate geometry, corresponds to the limit $W \to \infty$. In this limit, the form factors, defined in (2.18) and (2.19) become

$$f_1(\alpha, \delta, t) = \frac{24}{\pi^2}\int_0^\infty q\, dq\, G(q, \alpha, \delta)[1 - \tanh q] \cos tq, \tag{3.1}$$

$$f_2(\alpha, \delta, t) = \frac{12}{\pi^2}\int_0^\infty q\, dq\, G(q, \alpha, \delta)[\coth q - 1] \cos tq. \tag{3.2}$$

We have ignored the formal distinction between primed and unprimed variables. Note that $\Delta f \to 0$ as $W \to \infty$.

These integrals can be evaluated analytically for the case of a hard-edged beam. We therefore neglect the finite drop-off range, letting $\delta \to 0$. f_1 and f_2 can then be written as

$$f_1(\alpha, t) = \frac{48}{\pi^2\alpha}\int_0^\infty dq \sin \alpha q \cos tq \frac{e^{-2q}}{1+e^{-2q}}, \tag{3.3}$$

and

$$f_2(\alpha, t) = \frac{24}{\pi^2\alpha}\int_0^\infty dq \sin \alpha q \cos tq \frac{e^{-2q}}{1-e^{-2q}}. \tag{3.4}$$

These integrals can be done analytically, using the expansions

$$\frac{1}{1 \pm e^{-2q}} = \sum_{n=0}^{\infty} (\mp 1)^n e^{-2nq}. \tag{3.5}$$

Interchanging the sum over n and the integration over q, we can carry out both operations analytically. We thus obtain

$$f_1(\alpha, t) = \frac{24}{\pi^2}\left[\frac{1}{\alpha^2 - t^2} - \frac{\pi}{4\alpha}\left(\frac{1}{\sinh \frac{1}{2}\pi(\alpha+t)} + \frac{1}{\sinh \frac{1}{2}\pi(\alpha-t)}\right)\right], \tag{3.6}$$

$$f_2(\alpha, t) = \frac{12}{\pi^2}\left[-\frac{1}{\alpha^2 - t^2} + \frac{\pi}{4\alpha}\left(\frac{1}{\tanh \frac{1}{2}\pi(\alpha+t)} + \frac{1}{\tanh \frac{1}{2}\pi(\alpha-t)}\right)\right]. \tag{3.7}$$

These functions are defined to have the values

$$f_1(0, 0) = f_2(0, 0) = 1. \tag{3.8}$$

Furthermore their asymptotic behavior ($\alpha \to \infty$) at $t = 0$ can readily be obtained:

$$f_1(\alpha, 0) \to \frac{24}{\pi^2\alpha^2}, \tag{3.9}$$

$$f_2(\alpha, 0) \to \frac{6}{\pi\alpha}. \tag{3.10}$$

Thus, for large α, f_1 and f_2 both tend to zero, but f_2

slower than f_1. In fact, the image-tune-shifts due to electric and magnetic boundaries will, for large beam widths, a, go like

$$(\Delta\nu)_{\text{el}} \to \frac{1}{a^2}, \tag{3.11}$$

$$(\Delta\nu)_{\text{mag}} \to \frac{1}{ag}. \tag{3.12}$$

To study the ν-variation across the beam, we consider wide beams, α large, and let t approach α. Then near the positive edge (t near α), we can write

$$f_1(\alpha, t) \simeq \frac{6}{\pi\alpha}\left[\frac{2}{\pi(\alpha-t)} - \frac{1}{\sinh \frac{1}{2}\pi(\alpha-t)}\right], \tag{3.13}$$

$$f_2(\alpha, t) \simeq \frac{3}{\pi\alpha}\left[1 + \frac{1}{\tanh \frac{1}{2}\pi(\alpha-t)} - \frac{2}{\pi(\alpha-t)}\right]. \tag{3.14}$$

Consider first f_2: for t near α and α sufficiently large, (3.14) gives

$$f_2(\alpha, t) \simeq \frac{3}{\pi\alpha}. \tag{3.15}$$

Also f_2 is monotonic as a function of t in the region near α. Thus, from (3.10) and (3.15) we have that $(\Delta\nu)_{\text{im}}$ (magnetic) decreases from the center to the edge by the ratio

$$\frac{(\Delta\nu)_{\text{im}}\,(\text{magnetic, edge})}{(\Delta\nu)_{\text{im}}\,(\text{magnetic, center})} = \frac{f_2(\alpha, \alpha)}{f_2(\alpha, 0)} \simeq \frac{1}{2}. \tag{3.16}$$

Note that the $1/\alpha$ drop-off for f_2 is valid both at the center and the edge of the beam. For f_1, the situation is quite different. From (3.6) we can deduce that at the beam edge, $t \to \alpha$, and for sufficiently large α, the drop-off is like $1/\alpha^2$:

$$f_1(\alpha, \alpha) \simeq \frac{6}{\pi^2\alpha^2}. \tag{3.17}$$

Comparing this with (3.9), we have

$$\frac{(\Delta\nu)_{\text{im}}\,(\text{electric, edge})}{(\Delta\nu)_{\text{im}}\,(\text{electric, center})} = \frac{f_1(\alpha, \alpha)}{f_1(\alpha, 0)} \simeq \frac{1}{4}. \tag{3.18}$$

That is, the ν-shift at the beam edge is only one-fourth of its value at the center. But note that the drop-off is still like $1/\alpha^2$. However, from (3.13) we can see that if α is large enough, f_1 will start to increase as t approaches α, reach a peak and then decline to its value at $t = \alpha$.

It is easy to show that the peak of (3.13) occurs at

$$t_p = \alpha - \frac{2}{\pi}u_p \approx \alpha - 1.6, \tag{3.19}$$

and has the value

$$f_1(\alpha, t_p) \simeq \frac{6}{\pi\alpha}\left(\frac{1}{u_p} - \frac{1}{\sinh u_p}\right) \simeq \frac{3}{2\pi\alpha}. \tag{3.20}$$

Thus, although the drop-off in f_1 is like $1/\alpha^2$ at the center and edge of the beam, the behavior at t_{peak} is slower, like $1/\alpha$. In other words, at the peak,

$$(\Delta\nu)_{\text{el}} \to \frac{1}{ah}. \tag{3.21}$$

In general, if α is not too large, f_1, as well as f_2, will be monotonically decreasing as t varies from zero (beam center) to α (beam edge). The ratios of the electric and magnetic ν-shifts at the edge to those at the center can be written

$$\frac{f_1(\alpha, \alpha)}{f_1(\alpha, 0)} = \frac{1}{4}\frac{(1 - \pi\alpha/\sinh \pi\alpha)}{(1 - \pi\alpha/2\sinh \frac{1}{2}\pi\alpha)}, \tag{3.22}$$

and

$$\frac{f_2(\alpha, \alpha)}{f_2(\alpha, 0)} = \frac{1}{4}\frac{(1 - \pi\alpha/\tanh \pi\alpha)}{(1 - \pi\alpha/2\tanh \frac{1}{2}\pi\alpha)}. \tag{3.23}$$

These expressions are obtained from (3.6) and (3.7), respectively, and are consistent with the asymptotic expressions (3.18) and (3.16). These functions are plotted in Figure 3, where the f_1 ratio is compared with the expressions given in Refs. 2 and 5, which are

$$\frac{f_1(\alpha, \alpha)}{f_1(\alpha, 0)}[\text{Ref. 2}] = \frac{1}{1 + \frac{1}{2}\alpha^2} \tag{3.24}$$

and

$$\frac{f_1(\alpha, \alpha)}{f_1(\alpha, 0)}[\text{Ref. 5}] = 1 - \tfrac{3}{4}\alpha^2. \tag{3.25}$$

We have considered effects arising from a wide beam with uniform charge density. The notion behind such a configuration is an attempt to reduce the vertical space-charge ν-shift due to images by spreading out the charge horizontally. This is most efficiently accomplished by keeping the horizontal density uniform. However, the uniformity of the distribution, coupled naturally with the 'rapid' fall-off of the density at the beam edge, leads to a peaking of the ν-shift near the edge. This effect is

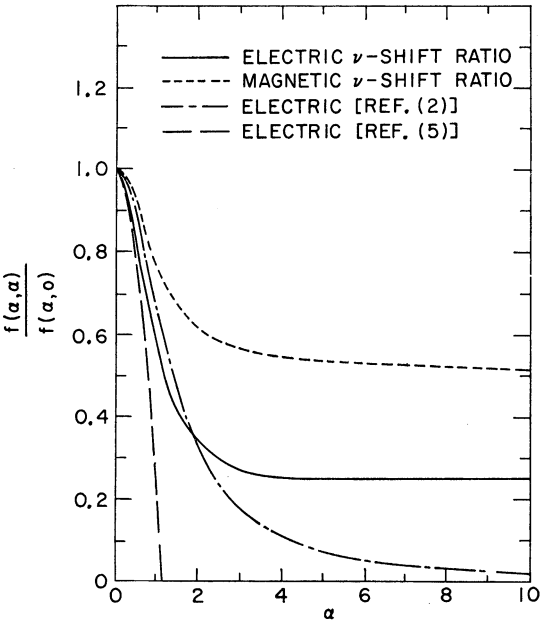

FIGURE 3 ν-shift ratios. The curves are contributions to the ratio of the ν-shift at the center of a beam to the ν-shift at the beam edge. A hard-edged beam is assumed and the chamber width is taken to be infinite. The variable α is the ratio of beam width to chamber height (or magnet gap). See Section 3, Eqs. (3.22), (3.23), (3.24), and (3.25).

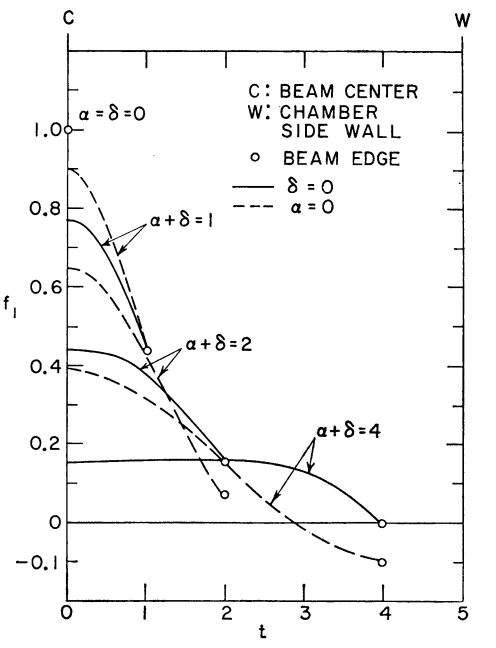

FIGURE 4 Electric form factor (f_1) as a function of position along the beam (t). All parameters are taken with respect to the chamber height, h. The chamber sidewall position is given by $\omega = 0.2$.

intrinsic in the sense that it can be removed only by making the effective beam width smaller. It should be recognized that softening the edge of the distribution, i.e., producing a slow fall-off is, in essence, decreasing the effective beam width. That is, for a given physical extent of the beam, a slower drop-off of charge density means a larger density at the center. We will consider these points further in the next section.

4. NUMERICAL RESULTS FOR FINITE SIDEWALLS AND SOFT DENSITY DISTRIBUTION FALL-OFF

We have previously considered the case of a hard-edged density distribution function ($\delta = 0$) with the chamber sidewalls at infinity ($W \to \infty$). These conditions allowed us to obtain the form factors f_1 and f_2 in closed form, i.e., (3.6) and (3.7). When W is finite and $\delta \neq 0$, we must use numerical methods. In our computations, we will use (2.18), (2.19), and (2.25). No distinction will be made between primed

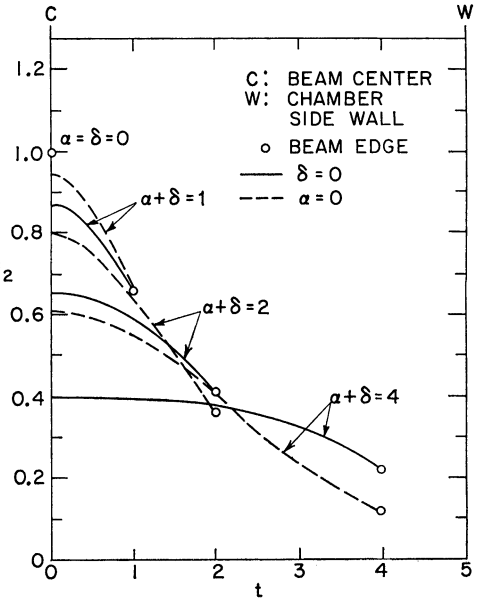

FIGURE 5 Magnetic form factor (f_2) as a function of position along the beam (t). All parameters are taken with respect to the gap height, g. The chamber sidewall position is given by $\omega = 0.2$.

and unprimed variables. Some care must therefore be exercised in translating the results to actual ν-shifts.

In Figure 4 we plot the electric form factor, f_1, as a function of horizontal position along the beam, i.e., as a function of t, for half beam sizes of 4, 2, and 1 times the half-chamber-height, and for a chamber width five times the height ($\omega = 0.2$). Equivalent plots for f_2 are shown in Figure 5.

Focusing on the $\delta = 0$ curves, we notice the decline in f at the beam center ($t = 0$) as α increases. This corresponds simply to the fact that spreading out the charge, i.e., reducing the density, decreases the ν-shift at the beam center. The effect is adequately described by (3.6) and (3.7) with $t = 0$. For large α, the asymptotic expressions (3.9) and (3.10) can be used. In the $\alpha = 4$ curve (Figure 4), we see the peaking effect (a very mild one for this α) at about 1.9 units from the beam edge. The theoretical value is 1.6 units. The shift is due to the nearby presence of the chamber wall.

Another effect of the chamber wall is to cause a more rapid fall-off in f_1. [There is no effect on f_2, even with the wall this close. This is, in a sense, a vindication of our simplifying assumption in deriving the force, Eq. (2.9), that the normal component of the magnetic field vanishes at the sidewalls, which is, of course, approximately true sufficiently far from the beam.] In fact, for the $\alpha = 4$ case, f_1 becomes negative at the beam edge. Thus, if the chamber walls are close to the edges of the beam, the expressions (3.18) and (3.22) giving the ratio of ν-shift at the edge to that at the center are not valid. The spread in ν-shifts across the beam actually becomes larger than the ν-shift at the center. This condition is more pronounced if one also considers the peaking effect. For the other $\delta = 0$ curves, (3.22) and (3.23) apply and agree with the numerical results.

In Figures 4 and 5, we can also see the influence of softening the fall-off of the charge distribution. We consider the extreme case of $\alpha = 0$. As can be seen, the three main effects are: (1) an increase in the ν-shift at the beam center; (2) a more rapid fall-off, meaning an increase in the spread of ν-shifts across the beam; and (3) a disappearance in f_1 of the peaking effect which is predominantly due to the hard-edge of the $\delta = 0$ case.

To show the peaking effect more clearly, we plot in Figure 6 the electric form factor, f_1, for beam sizes up to eight times the chamber height, taking a chamber width ten times the chamber height ($\omega = 0.1$).

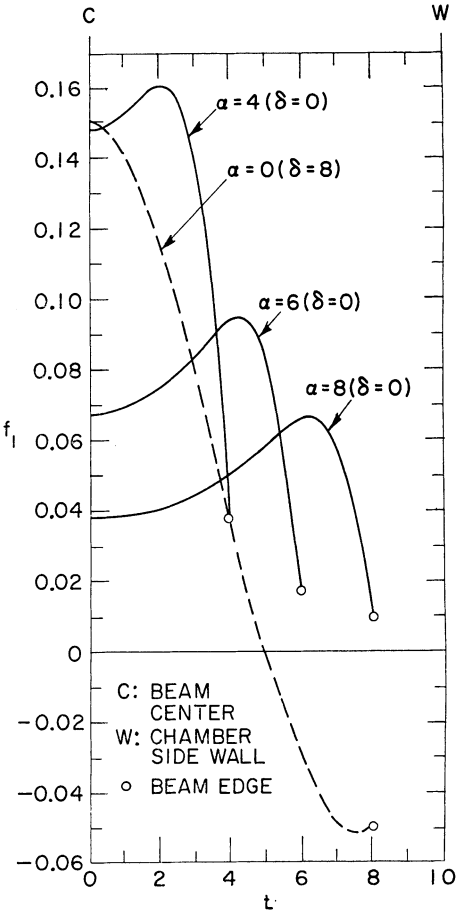

FIGURE 6 Peaking effect in electric form factor (f_1). The chamber sidewall is at a position 10 times the height ($\omega = 0.1$).

5. CONCLUSIONS

We have considered the effect of the distribution of charge in a beam of particles on the space-charge ν-shift. At high energy, the major contribution to the space-charge ν-shift comes from the image fields created by the presence of metallic and ferromagnetic boundaries. For beams small with respect to chamber and magnet dimensions, a point source treatment of the beam is adequate. However, when the beam width is comparable to or greater than the chamber height, the distribution of charge cannot be neglected. To study this effect, we have used a

rectangular geometry, assuming a conducting vacuum chamber, a parallel plate ferromagnetic surface and a ribbon beam.

Our conclusions are as follows:

1) The spreading of charge in a ribbon beam does indeed substantially reduce the space-charge ν-shift due to images. We have shown, however, that for a beam size, a, larger than the chamber height, h, the shift goes as $1/ah$, and not $1/a^2$. That is, the dependence on h persists.

2) For a wide, hard-edged beam, we have found that the electric image contribution reduces the tune shift at the beam edge to 25 per cent of its value at the center. For the magnetic image contribution, this reduction is 50 per cent. The two tune shift ratios (center to edge) are not the same (see, in this regard, Ref. 2). We have computed these ratios for a hard-edged beam and compared the electric contribution with the approximate expressions in Refs. 2 and 5.

3) We have discussed the influence of nearby chamber sidewalls and a slow drop-off of the charge density distribution. We have found that the main effect is an increase in the spread of ν-shifts across the width of the beam, even though a sufficiently slow variation of the charge density distribution removes the 'peaking effect' of the electric form factor.

ACKNOWLEDGMENTS

The authors would like to thank K. Jellett for performing all the numerical computations and Dr. E. D. Courant for valuable discussions.

REFERENCES

1. L. J. Laslett, *Proc. 1963 Summer Study on Storage Rings, Accelerators and Experimentation at Super-High Energies, Brookhaven National Laboratory* (BNL 7534), p. 324.
2. B. Zotter, CERN Rept., CERN-ISR-TH/72-36 (1972).
3. M. Month and K. Jellett, *Nucl. Instrum. Methods*, **113,** 453 (1973).
4. '200 GeV Intersecting Storage Accelerators, ISABELLE, A Preliminary Design Study,' BNL Informal Rept. BNL 16716 (1972).
5. R. L. Gluckstern, BNL Accelerator Dept. Informal Rept. CRISP 72–33 (1972).
6. A vertical displacement of the beam contributes to the 'coherent' ν-shift. See, in this regard, L. J. Laslett and L. Resegotti, *Proc. 6th Int. Conf. on High Energy Accelerators, Cambridge, Mass.*, 1967, p. 150.
7. For derivations of this result, see, for example, B. Zotter, CERN Rept., CERN-ISR-TH/72–8 (1972), or Ref. 6.

Received 16 August 1973